Geomechanics and Engineering, *Vol. 32, No. 6 (2023) 615-625*
https://doi.org/10.12989/gae.2023.32.6.615

Thermal post-buckling behavior of GPLRMF cylindrical shells with initial geometrical imperfection

Yi-Wen Zhang, Gui-Lin She*, Lei-Lei Gan and Yin-Ping Li

College of Mechanical and Vehicle Engineering, Chongqing University, Chongqing 400044, China

(*Received December 20, 2022, Revised February 17, 2023, Accepted February 20, 2023*)

Abstract. Initial geometrical imperfection is an important factor affecting the structural characteristics of plate and shell structures. Studying the effect of geometrical imperfection on the structural characteristics of cylindrical shell is beneficial to explore the thermal post-buckling response characteristics of cylindrical shell. Therefore, we devote to investigating the thermal post-buckling behavior of graphene platelets reinforced mental foam (GPLRMF) cylindrical shells with geometrical imperfection. The properties of GPLRMF material with considering three types of graphene platelets (GPLs) distribution patterns are introduced firstly. Subsequently, based on Donnell nonlinear shell theory, the governing equations of cylindrical shell are derived according to Eulerian-Lagrange equations. Taking into account two different boundary conditions namely simply supported (S-S) and clamped supported (C-S), the Galerkin principle is used to solve the governing equations. Finally, the impact of initial geometrical imperfections, the GPLs distribution types, the porosity distribution types, the porosity coefficient as well as the GPLs mass fraction on the thermal post-buckling response of the cylindrical shells are analyzed.

Keywords: cylindrical shells; Galerkin' method; graphene platelet; initial geometrical imperfection; metal foams; thermal post-buckling

1. Introduction

GPLRMF refers to carbon materials with nanoscale pores on two-dimensional substrates. Compared with the single GPLs material, GPLRMF not only retains the original excellent properties of graphene, but also has the excellent physical and chemical properties such as high specific area and high transmission efficiency. Therefore, GPLs has a wide range of applications, and it has very important application value and research significance in the new energy, new materials, energy storage, catalysis and other fields, there are a lot of literatures on it. For example, Van Doan *et al.* (2022) investigated the nonlinear buckling of functionally graded graphene reinforced composite (FG-GRC) annular shells using the Donnell's shell theory (DST). Based on the higher-order shear deformation theory (HSDT), Ramezani *et al.* (2022) analyzed the nonlinear behavior of FG-GRC cylindrical shells. Allahkarami and Tohidi (2022) illustrated the thermal post-buckling behavior of FG-GRC plates. Phuong *et al.* (2022) employed the HSDT to research the nonlinear thermal post-buckling response of FG-GRC plate. Saiah *et al.* (2022) discussed the free vibration response of FG-GRC plate using the first order shear deformation theory (FSDT). Kolahchi *et al.* (2019) researched the influence of movable boundary condition on the thermal post-buckling response of quadrilateral graphene platelets by HSDT. Ebrahimi *et al.* (2020) applied the HSDT to explain the thermal vibration phenomenon of GPRC plate. Gholami and Ansari (2019) investigated the nonlinear free vibration behavior of FG-GRC rectangular plate using the Von Karman method. Phuong *et al.* (2021) researched the nonlinear thermal post-buckling behavior of FG-GRC laminated shells on an elastic foundation using the DST. With the aid of the strain gradient theory, the nonlinear bending response of GPLRMF micro/nano beam is investigated by Sahmani *et al.* (2018).

Thermal buckling is a common failure type of plate-shell structures in engineering applications (Basha 2022, Eltaher *et al.* 2019a, b, Akbari *et al*. 2015, Bagherizadeh *et al.* 2012, Hendi *et al.* 2022, Asadi *et al.* 2016, Melaibari *et al.* 2023, Torabi *et al.* 2013, Boroujerdy *et al.* 2014, Mohamed *et al.* 2021, Alazwari *et al.* 2021, Assie *et al.* 2023, Babaei 2021, 2022a, b, Javani *et al.* 2020, Quyen *et al.* 2021, Mirjavadi *et al.* 2020, Nguyen *et al.* 2021, Aris and Ahmadi 2022, Malikan *et al.* 2019, 2022). Many scientists have carried out a lot of research on this kind of problems. For example, Shahgholian *et al.* (2020) researched the buckling phenomenon of GPLRMF cylindrical shells using the FSDT. Shahgholian-Ghahfarokhi *et al.* (2021) operated the FSDT to study the buckling response of GPLRMF cylindrical shells under external pressure. Kiani (2020) analyzed the thermal buckling behaviors of GPRC laminated plate based on the FSDT. Nguyen *et al.* (2021) applied the DST to study the thermal post buckling behavior of FG-GRC cylindrical shells. With the help of the FSDT, Mahani *et al.* (2020) illustrated the thermal buckling behaviors of FG-GRC shells. Phuong *et al.* (2020) researched the nonlinear buckling and post-buckling characteristics of FG-GRC cylindrical shells in thermal environment by the DST.

*Corresponding author, Professor
E-mail: sheguilin@cqu.edu.cn

ISSN: 2005-307X (Print), 2092-6219 (Online)

Initial geometrical imperfection is inevitable in the design and manufacture of engineering structures, and its existence will greatly reduce the stiffness and strength of the structure. Therefore, it is necessary to research the impact of initial geometrical imperfection on the mechanical behavior of components. Salehi *et al.* (2022) investigated the nonlinear resonance response of GPLRMF cylindrical shells with initial geometrical imperfection under external loading. Through numerical analysis, Martins *et al.* (2021) discussed the post-buckling response of beam under distorted conditions. Krasovsky and Evkin (2021) proposed an experimental model to analyze the pre- and post-buckling phenomena of initial geometrical imperfection shell. Dinis *et al.* (2021) studied the strength and post-buckling response of column with initial geometrical imperfection using finite element analysis (FEA). Zmuda-Trzebiatowski and Iwicki (2021) employed the vibration correlation techniques to study the influence of geometrical imperfections on the ultimate loading and buckling behavior of silo segments. Ming *et al.* (2021) deliberated the influence of geometrical imperfection on the energy absorption capacity of the tube using the numerical analysis. Ahmadi *et al.* (2021) applied the classical shell theory to research the nonlinear vibration behavior of stiffened FG doubly curved shell. Khaniki *et al.* (2022) used the von Karman method to analyze the effect of geometrical imperfection on the vibration characteristics of GPRC beam under different boundary conditions. Ismail *et al.* (2020) came up with the numerical model to illustrate the buckling response of geometrically imperfect cone columns. Kolakowski *et al.* (2020) proffered a finite element model to explain the nonlinear buckling behavior of thin-walled lip beams. Trang and Tung (2022) explored the influence of initial geometrical imperfection on the post-buckling behavior of carbon nanotube reinforced plates under external thermal loading. Ma *et al.* (2020) investigated the buckling response of cylindrical shells under external loads using the energy method. Yilmaz *et al.* (2020) used the classical shell theory to examine the stabilities of conical shells with initial geometrical imperfection subject to the external loads. Martins and Silvestre (2020) employed the nonlinear generalized beam theory to analyze the imperfection sensitivity of the cylindrical plate after buckling. Stawiarski *et al.* (2020) researched the mechanical properties of conical shells with concave convex imperfection on the bearing capacity by the FEA. Martins *et al.* (2019) studied the imperfection sensitivity and post-buckling response of the pipe under external loads using the NGBT. In addition, these years, a set of papers published by She and his collaborators (for example, Xu and She 2022, She and Ding 2023, She *et al.* 2022, She and Li 2022, She *et al.* 2021, Zhang *et al.* 2022, Zhang *et al.* 2023a, b, Zhang and She 2022, Lu *et al.* 2021, Ding and She 2021, Ding *et al.* 2022a, b, Chen *et al.* 2022a, b, She 2022, She 2020, She 2021, Zhao *et al.* 2022a, b, Zhang *et al.* 2021, Zhang and She 2023a, Zhang and She 2023b), but none of them examined such a topic in this paper.

To make a long story short, no papers examined nonlinear thermal stability of GPLRMF cylindrical shells with initial geometrical imperfection. It is known that geometrical imperfection has significant impact, in addition, for common engineering equipment, the existence of initial geometrical defects will significantly increase the probability of material damage during their service. Therefore, this paper focuses on analyzing the influence of initial geometrical imperfections on the thermal post-buckling response of cylindrical shells. The Galerkin method is applied to solve the governing equations with considering two different boundary conditions. In addition, the effects of several parameters on the post-thermal buckling behaviors are also investigated, including initial geometrical imperfections, porosity distribution types, porosity coefficient etc. By conducting this research, it is hoped to provide references for the thermal stability analysis of cylindrical shell structures in engineering practice.

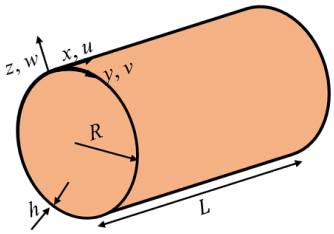

Fig. 1 A GPLRMF cylindrical shell

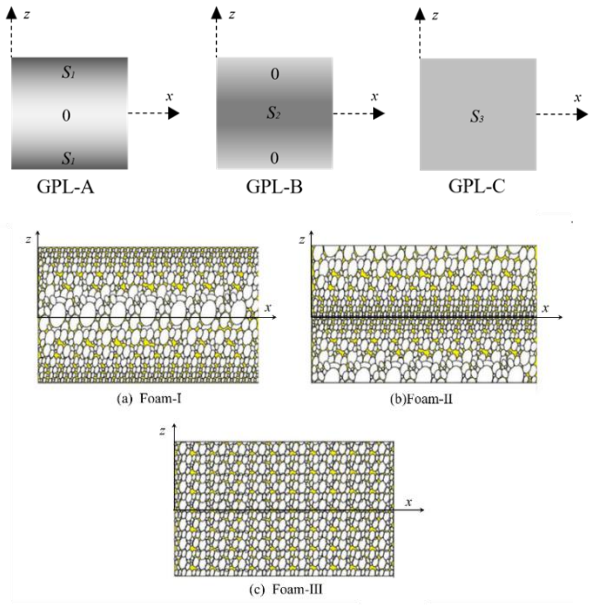

Fig. 2 Material attributes (Wang and Wu 2017)

2. Material properties

In this paper, we study the thermal post-buckling behavior of GPLRMF cylindrical shell, and the geometrical dimensions and coordinate system of the shell are shown in Fig. 1. The shell is affected by a uniform temperature field

ΔT. The density $\rho(z)$ of the shell is related to the density of GPLs and matrix, $\rho_{gpl}, \rho_M, e_{mi}(i=1,2,3)$ respectively represent GPLs' density, matrix' density, porosity coefficient are (Yang *et al.* 2017, Zhang and She 2023a)

$$\rho(z)=\begin{cases}\left\{\rho_{gpl}V_{gpl}+\rho_M\left(1-V_{gpl}\right)\right\}\left[1-\mathrm{e}_{m1}\cos\left(\pi z/h\right)\right],\\ \left(\text{Foam-}\mathrm{I}\right)\\ \left\{\rho_{gpl}V_{gpl}+\rho_M\left(1-V_{gpl}\right)\right\}\left\{1-\mathrm{e}_{m2}\left[1-\cos\left(\pi z/h\right)\right]\right\},\\ \left(\text{Foam-}\mathrm{II}\right)\\ \left\{\rho_{gpl}V_{gpl}+\rho_M\left(1-V_{gpl}\right)\right\}\mathrm{e}_{m3},\\ \left(\text{Foam-}\mathrm{III}\right)\end{cases} \tag{1}$$

The thermal expansion coefficient $\alpha(z)$ is also related to the thermal expansion coefficients of GPLs α_{gpl}, and matrix α_M, and (Yang *et al.* 2017, Gao *et al.* 2018, Zhang and She 2023a, Wang *et al*. 2019)

$$\alpha(z)=\begin{cases}\left\{\alpha_{gpl}V_{gpl}+\alpha_M\left(1-V_{gpl}\right)\right\}\left[1-\mathrm{e}_{m1}\cos\left(\pi z/h\right)\right],\\ \left(\text{Foam-}\mathrm{I}\right)\\ \left\{\alpha_{gpl}V_{gpl}+\alpha_M\left(1-V_{gpl}\right)\right\}\left\{1-\mathrm{e}_{m2}\left[1-\cos\left(\pi z/h\right)\right]\right\},\\ \left(\text{Foam-}\mathrm{II}\right)\\ \left\{\alpha_{gpl}V_{gpl}+\alpha_M\left(1-V_{gpl}\right)\right\}\mathrm{e}_{m3},\\ \left(\text{Foam-}\mathrm{III}\right)\end{cases} \tag{2}$$

For all the foam types, the Poisson's ratio $\mu(z)$ is also related to the Poisson's ratio of GPLs μ_{gpl} and matrix μ_M, and (Yang *et al.* 2017, Gao *et al*. 2018, Zhang and She 2023a)

$$\alpha(z)=\mu_{gpl}V_{gpl}+\mu_M\left(1-V_{gpl}\right) \tag{3}$$

The effective elastic modulus $E(z)$ is also related to the elastic modulus of GPLs E_{gpl} and matrix E_M,which has the following expression (Gao *et al.* 2018, Zhang and She 2023a)

$$E(z)=\begin{cases}\left\{\frac{3}{8}\delta_1E_M+\frac{5}{8}\delta_2E_M\right\}\left[1-\mathrm{e}_1\cos\left(\pi z/h\right)\right],\\ \left(\text{Foam-}\mathrm{I}\right)\\ \left\{\frac{3}{8}\delta_1E_M+\frac{5}{8}\delta_2E_M\right\}\left\{1-\mathrm{e}_2\left[1-\cos\left(\pi z/h\right)\right]\right\},\\ \left(\text{Foam-}\mathrm{II}\right)\\ \left\{\frac{3}{8}\delta_1E_M+\frac{5}{8}\delta_2E_M\right\}\mathrm{e}_3,\left(\text{Foam-}\mathrm{III}\right)\end{cases} \tag{4}$$

In which, $\delta_1=\left(\frac{1+\zeta_L\frac{\left(E_{gpl}/E_M\right)-1}{\left(E_{gpl}/E_M\right)+2\left(l_{gpl}/h_{gpl}\right)}V_{gpl}}{1-\frac{\left(E_{gpl}/E_M\right)-1}{\left(E_{gpl}/E_M\right)+2\left(l_{gpl}/h_{gpl}\right)}V_{gpl}}\right),\delta_2=\left(\frac{1+\zeta_W\frac{\left(E_{gpl}/E_M\right)-1}{\left(E_{gpl}/E_M\right)+2\left(w_{gpl}/h_{gpl}\right)}V_{gpl}}{1-\frac{\left(E_{gpl}/E_M\right)-1}{\left(E_{gpl}/E_M\right)+2\left(w_{gpl}/h_{gpl}\right)}V_{gpl}}\right)$.

The symbol V_{gpl} appeared in Eqs. (1)-(4) is the GPLs weight fraction, which can be described as (Zhang and She 2023a)

$$V_{GPL}=\begin{cases}\left[1-\lambda(z)\right]Si_1,\ \left(\text{GPL-A}\right)\\ \lambda(z)Si_2,\ \left(\text{GPL-B}\right)\\ Si_3,\ \left(\text{GPL-C}\right)\end{cases} \tag{5}$$

In which, the coefficients Si_1, Si_2 and Si_3 can refer to (Wang *et al*. 2020). And the porosity coefficients $e_m(i=1,2,3)$ can be determined by the following expression (Zhang and She 2023a)

$$\int_0^{\frac{h}{2}}\sqrt{1-e_1\lambda(z)}dz=\int_0^{\frac{h}{2}}\sqrt{1-e_2\lambda(z)}dz=\int_0^{\frac{h}{2}}\sqrt{e_3}dz \tag{6}$$

3. Governing equations

Based on Donnell nonlinear shell theory, the components for the strain can be written as (Zhang and She 2023a)

$$\begin{aligned}\varepsilon_x&=\frac{\partial u}{\partial x}+\frac{1}{2}\left(\frac{\partial w}{\partial x}\right)^2+\frac{\partial w}{\partial x}\frac{\partial w^*}{\partial x}-z\frac{\partial^2 w}{\partial x^2},\\ \varepsilon_y&=\frac{\partial v}{\partial y}+\frac{1}{2}\left(\frac{\partial w}{\partial y}\right)^2+\frac{w}{R}+\frac{\partial w}{\partial y}\frac{\partial w^*}{\partial y}-z\left(\frac{\partial^2 w}{\partial y^2}-\frac{1}{R}\frac{\partial v}{\partial y}\right),\\ \gamma_{xy}&=\frac{\partial v}{\partial x}+\frac{\partial u}{\partial y}+\frac{\partial w}{\partial x}\frac{\partial w}{\partial y}+\frac{\partial w}{\partial x}\frac{\partial w^*}{\partial y}+\frac{\partial w}{\partial y}\frac{\partial w^*}{\partial x}\\ &-2z\left(\frac{\partial^2 w}{\partial x\partial y}-\frac{1}{R}\frac{\partial v}{\partial x}\right).\end{aligned} \tag{7}$$

Herein, w^* is the initial geometrical imperfection, using Eq. (7), the relationship between stress and strain is as follows (Zhang and She 2023b)

$$\begin{aligned}\sigma_x&=Q_{11}\varepsilon_x+Q_{12}\varepsilon_y\text{-}\alpha(z)\Delta T\\ \sigma_y&=Q_{12}\varepsilon_x+Q_{22}\varepsilon_y\text{-}\alpha(z)\Delta T\\ \sigma_{xy}&=Q_{66}\gamma_{xy}\end{aligned} \tag{8}$$

In which, ΔT is the uniform temperature change, and the stiffness coefficients $Q_{ij}(ij=11,12,22)$ are (Zhang and She 2023b)

$$Q_{11}=Q_{22}=\frac{E(z)}{1-v^2},Q_{12}=\frac{vE(z)}{1-v^2},Q_{22}=\frac{E(z)}{2(1+v)}. \tag{9}$$

At this time, the control equations have the following expressions

$$\begin{aligned}&\frac{\partial N_x}{\partial x}+\frac{\partial N_{xy}}{\partial y}=0,\\ &\frac{\partial N_{xy}}{\partial x}+\frac{\partial N_y}{\partial y}+\frac{1}{R}\left(\frac{2\partial M_{xy}}{\partial x}+\frac{\partial M_y}{\partial y}\right)=0,\\ &\frac{\partial^2 M_x}{\partial x^2}+2\frac{\partial^2 M_{xy}}{\partial x\partial y}+\frac{\partial^2 M_y}{\partial y^2}-\frac{N_y}{R}+N_x\frac{\partial^2 w}{\partial x^2}+2N_{xy}\frac{\partial^2 w}{\partial x\partial y}\\ &+N_y\frac{\partial^2 w}{\partial y^2}=0.\end{aligned} \tag{10}$$

The internal forces and couples have the following

expressions

$$\begin{bmatrix} N_x \\ N_y \\ N_{xy} \\ M_x \\ M_y \\ M_{xy} \end{bmatrix} = \begin{bmatrix} A_{11} & A_{12} & 0 & B_{11} & B_{12} & 0 \\ A_{12} & A_{22} & 0 & B_{12} & B_{22} & 0 \\ 0 & 0 & A_{66} & 0 & 0 & B_{66} \\ B_{11} & B_{12} & 0 & D_{11} & D_{12} & 0 \\ B_{12} & B_{22} & 0 & D_{12} & D_{22} & 0 \\ 0 & 0 & B_{66} & 0 & 0 & D_{66} \end{bmatrix}$$

$$\times \begin{bmatrix} \dfrac{\partial u}{\partial x}+\dfrac{1}{2}\left(\dfrac{\partial w}{\partial x}\right)^2+\dfrac{\partial w}{\partial x}\dfrac{\partial w^*}{\partial x}, \\ \dfrac{\partial v}{\partial y}+\dfrac{1}{2}\left(\dfrac{\partial w}{\partial y}\right)^2+\dfrac{w}{R}+\dfrac{\partial w}{\partial y}\dfrac{\partial w^*}{\partial y}, \\ \dfrac{\partial v}{\partial x}+\dfrac{\partial u}{\partial y}+\dfrac{\partial w}{\partial x}\dfrac{\partial w}{\partial y}+\dfrac{\partial w}{\partial x}\dfrac{\partial w^*}{\partial y}+\dfrac{\partial w}{\partial y}\dfrac{\partial w^*}{\partial x}, \\ \dfrac{\partial^2 w}{\partial x^2}, \dfrac{\partial^2 w}{\partial y^2}-\dfrac{1}{R}\dfrac{\partial v}{\partial y}, \dfrac{\partial^2 w}{\partial x\partial y}-\dfrac{1}{R}\dfrac{\partial v}{\partial x} \end{bmatrix}^T - \begin{bmatrix} N^T \\ N^T \\ 0 \\ 0 \\ 0 \end{bmatrix} \tag{11}$$

In which (Zhang and She 2023a)

$$\left[A_{ij}, B_{ij}, D_{ij}\right] = \int_{-\frac{h}{2}}^{\frac{h}{2}} \left[1, z, z^2\right] Q_{ii}(z) dz,\ ij = (11,12,22,66). \tag{12}$$

Using Eq. (11), the equations of motion become

$$\begin{aligned} & A_{11}\frac{\partial^2 u}{\partial x^2}+A_{66}\frac{\partial^2 u}{\partial y^2}+\left[A_{12}+A_{66}+\frac{1}{R}\left(B_{12}+2B_{66}\right)\right]\frac{\partial^2 v}{\partial x\partial y} \\ & +\frac{A_{12}}{R}\frac{\partial w}{\partial x}-B_{11}\frac{\partial^3 w}{\partial x^3}-\left(B_{12}+2B_{66}\right)\frac{\partial^3 w}{\partial x\partial y^2} \\ & +A_{11}\left(\frac{\partial^2 w}{\partial x^2}\frac{\partial w^*}{\partial x}+\frac{\partial w}{\partial x}\frac{\partial^2 w^*}{\partial x^2}\right)+A_{12}\left(\frac{\partial^2 w}{\partial x\partial y}\frac{\partial w^*}{\partial y}+\frac{\partial w}{\partial y}\frac{\partial^2 w^*}{\partial x\partial y}\right) \\ & +A_{66}\left(\frac{\partial^2 w}{\partial x\partial y}\frac{\partial w^*}{\partial y}+\frac{\partial w}{\partial y}\frac{\partial^2 w^*}{\partial x\partial y}+\frac{\partial^2 w}{\partial y^2}\frac{\partial w^*}{\partial x}+\frac{\partial^2 w^*}{\partial y^2}\frac{\partial w}{\partial x}\right) \\ & +A_{11}\frac{\partial w}{\partial x}\frac{\partial^2 w}{\partial x^2}+A_{12}\frac{\partial w}{\partial y}\frac{\partial^2 w}{\partial x\partial y}+A_{66}\left(\frac{\partial^2 w}{\partial y^2}\frac{\partial w}{\partial x}+\frac{\partial^2 w}{\partial x\partial y}\frac{\partial w}{\partial y}\right)=0 \end{aligned} \tag{13}$$

$$\begin{aligned} & \left[A_{66}+A_{12}+\frac{1}{R}\left(2B_{66}+B_{12}\right)\right]\frac{\partial^2 u}{\partial x\partial y} \\ & +\left[A_{66}+\frac{1}{R}\left(4B_{66}+\frac{4}{R}D_{66}\right)\right]\frac{\partial^2 v}{\partial x^2} \\ & +\left[A_{22}+\frac{1}{R}\left(2B_{22}+\frac{1}{R}D_{22}\right)\right]\frac{\partial^2 v}{\partial y^2} \\ & -\left[2B_{66}+B_{12}+\frac{1}{R}\left(4D_{66}+D_{12}\right)\right]\frac{\partial^3 w}{\partial x^2\partial y} \\ & +\frac{1}{R}\left(A_{22}+\frac{B_{22}}{R}\right)\frac{\partial w}{\partial y}-\left(B_{22}+\frac{1}{R}D_{22}\right)\frac{\partial^3 w}{\partial y^3} \\ & +\left(A_{66}+\frac{B_{66}}{R}\right)\left(\frac{\partial^2 w^*}{\partial x^2}\frac{\partial w}{\partial y}+\frac{\partial w^*}{\partial x}\frac{\partial^2 w}{\partial x\partial y}+\frac{\partial w}{\partial x}\frac{\partial^2 w^*}{\partial x\partial y}+\frac{\partial w^*}{\partial y}\frac{\partial^2 w}{\partial x^2}\right) \\ & +\left(A_{12}+\frac{B_{12}}{R}\right)\left(\frac{\partial^2 w}{\partial x\partial y}\frac{\partial w^*}{\partial x}+\frac{\partial w}{\partial x}\frac{\partial^2 w^*}{\partial x\partial y}\right) \\ & +\left(A_{22}+\frac{B_{22}}{R}\right)\left(\frac{\partial^2 w}{\partial y^2}\frac{\partial w^*}{\partial y}+\frac{\partial w}{\partial y}\frac{\partial^2 w^*}{\partial y^2}\right) \\ & +\left(A_{66}+2\frac{B_{66}}{R}\right)\left(\frac{\partial^2 w}{\partial x^2}\frac{\partial w}{\partial y}+\frac{\partial w}{\partial x}\frac{\partial^2 w}{\partial x\partial y}\right) \\ & +\left(A_{12}+\frac{B_{12}}{R}\right)\frac{\partial^2 w}{\partial x\partial y}\frac{\partial w}{\partial x}+\left(A_{22}+\frac{B_{22}}{R}\right)\frac{\partial^2 w}{\partial y^2}\frac{\partial w}{\partial y}=0 \end{aligned} \tag{14}$$

$$\begin{aligned} & B_{11}\frac{\partial^3 u}{\partial x^3}+\left(2B_{66}+B_{12}\right)\frac{\partial^3 u}{\partial x\partial y^2}-\frac{A_{12}}{R}\frac{\partial u}{\partial x} \\ & +\left[B_{12}+2B_{66}+\frac{1}{R}\left(4D_{66}+D_{12}\right)\right]\frac{\partial^3 v}{\partial x^2\partial y}+\left(B_{22}+\frac{D_{22}}{R}\right)\frac{\partial^3 v}{\partial y^3} \\ & -\left(\frac{A_{22}}{R}+\frac{B_{22}}{R^2}\right)\frac{\partial v}{\partial y}+\frac{2B_{12}}{R}\frac{\partial^2 w}{\partial x^2}+\frac{2B_{22}}{R}\frac{\partial^2 w}{\partial y^2}-D_{11}\frac{\partial^4 w}{\partial x^4}-D_{22}\frac{\partial^4 w}{\partial y^4} \\ & -(2D_{12}+4D_{66})\frac{\partial^4 w}{\partial x^2\partial y^2}-\frac{A_{22}}{R^2}w \\ & +B_{11}\left(\frac{\partial^3 w}{\partial x^3}\frac{\partial w^*}{\partial x}+2\frac{\partial^2 w}{\partial x^2}\frac{\partial^2 w^*}{\partial x^2}+\frac{\partial^3 w^*}{\partial x^3}\frac{\partial w}{\partial x}\right) \\ & +B_{12}\left(\frac{\partial^3 w}{\partial x^2\partial y}\frac{\partial w^*}{\partial y}+2\frac{\partial^2 w}{\partial x\partial y}\frac{\partial^2 w^*}{\partial x\partial y}+\frac{\partial w}{\partial y}\frac{\partial^3 w^*}{\partial x^2\partial y}\right) \\ & +2B_{66}\left(\begin{array}{l}\dfrac{\partial w}{\partial y}\dfrac{\partial^3 w^*}{\partial x^2\partial y}+\dfrac{\partial^2 w^*}{\partial x^2}\dfrac{\partial^2 w}{\partial y^2}+2\dfrac{\partial^2 w}{\partial x\partial y}\dfrac{\partial^2 w^*}{\partial x\partial y} \\ +\dfrac{\partial^3 w}{\partial x\partial y^2}\dfrac{\partial w^*}{\partial x}+\dfrac{\partial^2 w}{\partial x^2}\dfrac{\partial^2 w^*}{\partial y^2}+\dfrac{\partial w^*}{\partial y}\dfrac{\partial^3 w}{\partial x^2\partial y}+\dfrac{\partial^3 w^*}{\partial x\partial y^2}\dfrac{\partial w}{\partial x}\end{array}\right) \\ & +B_{12}\left(\frac{\partial^3 w}{\partial x\partial y^2}\frac{\partial w}{\partial x}+2\frac{\partial^2 w}{\partial x\partial y}\frac{\partial^2 w^*}{\partial x\partial y}+\frac{\partial w}{\partial x}\frac{\partial^3 w^*}{\partial x\partial y^2}\right) \\ & +B_{22}\left(\frac{\partial^3 w}{\partial y^3}\frac{\partial w^*}{\partial y}+2\frac{\partial^2 w}{\partial y^2}\frac{\partial^2 w^*}{\partial y^2}+\frac{\partial^3 w^*}{\partial y^3}\frac{\partial w}{\partial y}\right) \\ & -\frac{A_{12}}{R}\frac{\partial w}{\partial x}\frac{\partial w^*}{\partial x}-\frac{A_{22}}{R}\frac{\partial w}{\partial y}\frac{\partial w^*}{\partial y}+B_{11}\left(\frac{\partial^3 w}{\partial x^3}\frac{\partial w}{\partial x}+\frac{\partial^2 w}{\partial x^2}\frac{\partial^2 w}{\partial x^2}\right) \\ & +B_{12}\left(\frac{\partial^3 w}{\partial x^2\partial y}\frac{\partial w}{\partial y}+\frac{\partial^2 w}{\partial x\partial y}\frac{\partial^2 w}{\partial x\partial y}\right)+A_{22}\frac{\partial w}{\partial y}\frac{\partial w^*}{\partial y}\frac{\partial^2 w}{\partial y^2} \\ & +2B_{66}\left(\frac{\partial^3 w}{\partial x^2\partial y}\frac{\partial w}{\partial y}+\frac{\partial^2 w}{\partial x^2}\frac{\partial^2 w}{\partial y^2}+\frac{\partial^2 w}{\partial x\partial y}\frac{\partial^2 w}{\partial x\partial y}+\frac{\partial w}{\partial x}\frac{\partial^3 w}{\partial x\partial y^2}\right) \\ & +B_{12}\left(\frac{\partial^3 w}{\partial x\partial y^2}\frac{\partial w}{\partial x}+\frac{\partial^2 w}{\partial x\partial y}\frac{\partial^2 w}{\partial x\partial y}\right)+B_{22}\left(\frac{\partial^3 w}{\partial y^3}\frac{\partial w}{\partial y}+\frac{\partial^2 w}{\partial y^2}\frac{\partial^2 w}{\partial y^2}\right) \\ & -\frac{A_{12}}{2R}\left(\frac{\partial w}{\partial x}\right)^2-\frac{A_{22}}{2R}\left(\frac{\partial w}{\partial y}\right)^2+\frac{A_{12}}{R}w\frac{\partial^2 w}{\partial x^2}-B_{11}\left(\frac{\partial^2 w}{\partial x^2}\right)^2 \\ & -2B_{12}\frac{\partial^2 w}{\partial x^2}\frac{\partial^2 w}{\partial y^2}-4B_{66}\left(\frac{\partial^2 w}{\partial x\partial y}\right)^2+\frac{A_{22}}{R}w\frac{\partial^2 w}{\partial y^2}-B_{22}\left(\frac{\partial^2 w}{\partial y^2}\right)^2 \\ & +A_{11}\frac{\partial w}{\partial x}\frac{\partial w^*}{\partial x}\frac{\partial^2 w}{\partial x^2}+A_{12}\frac{\partial w}{\partial y}\frac{\partial w^*}{\partial y}\frac{\partial^2 w}{\partial x^2} \\ & +2A_{66}\left(\frac{\partial w^2}{\partial x\partial y}\frac{\partial w^*}{\partial x}\frac{\partial w}{\partial y}+\frac{\partial w^2}{\partial x\partial y}\frac{\partial w}{\partial x}\frac{\partial w^*}{\partial y}\right)+A_{12}\frac{\partial w}{\partial x}\frac{\partial w^*}{\partial x}\frac{\partial^2 w}{\partial y^2} \\ & +\frac{1}{2}A_{11}\left(\frac{\partial w}{\partial x}\right)^2\frac{\partial^2 w}{\partial x^2}+\frac{1}{2}A_{12}\left(\frac{\partial w}{\partial y}\right)^2\frac{\partial^2 w}{\partial x^2} \\ & +2A_{66}\frac{\partial^2 w}{\partial x\partial y}\frac{\partial w}{\partial x}\frac{\partial w}{\partial y}+\frac{1}{2}A_{12}\left(\frac{\partial w}{\partial x}\right)^2\frac{\partial^2 w}{\partial y^2}+\frac{1}{2}A_{12}\left(\frac{\partial w}{\partial y}\right)^2\frac{\partial^2 w}{\partial y^2} \\ & +A_{11}\frac{\partial u}{\partial x}\frac{\partial^2 w}{\partial x^2}+2A_{66}\frac{\partial^2 w}{\partial x\partial y}\frac{\partial u}{\partial y}+A_{12}\frac{\partial^2 w}{\partial y^2}\frac{\partial u}{\partial x} \\ & +\left(A_{12}+\frac{B_{12}}{R}\right)\frac{\partial v}{\partial y}\frac{\partial^2 w}{\partial x^2}+\left(2A_{66}+\frac{4A_{66}}{R}\right)\frac{\partial^2 w}{\partial x\partial y}\frac{\partial v}{\partial x} \\ & +\left(A_{22}+\frac{B_{22}}{R}\right)\frac{\partial^2 w}{\partial y^2}\frac{\partial v}{\partial y}=0. \end{aligned} \tag{15}$$

4. Solution method

In the following analysis, we consider two different boundary conditions, that is the displacement shape function satisfying simply supported and clamped edges has the following forms

$$\begin{cases} u=\sum_{m=1}^{\infty}\sum_{n=1}^{\infty}\mathbf{U}\cos\left(\frac{m\pi x}{L}\right)\cos\left(\frac{ny}{R}\right), \\ v=\sum_{m=1}^{\infty}\sum_{n=1}^{\infty}\mathbf{V}\sin\left(\frac{m\pi x}{L}\right)\sin\left(\frac{ny}{R}\right), \\ w=\sum_{m=1}^{\infty}\sum_{n=1}^{\infty}\mathbf{W}\sin\left(\frac{m\pi x}{L}\right)\cos\left(\frac{ny}{R}\right), \\ w^{*}=\sum_{m=1}^{\infty}\sum_{n=1}^{\infty}\mathbf{W}_1\sin\left(\frac{m\pi x}{L}\right)\cos\left(\frac{ny}{R}\right). \end{cases} \quad \text{(S-S)}$$

$$\begin{cases} u=\sum_{m=1}^{\infty}\sum_{n=1}^{\infty}\mathbf{U}\sin\left(\frac{2m\pi x}{L}\right)\cos\left(\frac{ny}{R}\right), \\ v=\sum_{m=1}^{\infty}\sum_{n=1}^{\infty}\mathbf{V}\left[1-\cos\left(\frac{2m\pi x}{L}\right)\right]\sin\left(\frac{ny}{R}\right), \\ w=\sum_{m=1}^{\infty}\sum_{n=1}^{\infty}\mathbf{W}\left[1-\cos\left(\frac{2m\pi x}{L}\right)\right]\cos\left(\frac{ny}{R}\right), \\ w^{*}=\sum_{m=1}^{\infty}\sum_{n=1}^{\infty}\mathbf{W}_1\left[1-\cos\left(\frac{2m\pi x}{L}\right)\right]\cos\left(\frac{ny}{R}\right). \end{cases} \quad \text{(C-S)} \tag{16}$$

Here $\mathbf{U}$, $\mathbf{V}$ and $\mathbf{W}$ are the undetermined coefficients. Substituting Eq. (16) into Eqs. (13)-(15), and then employing Galerkin' method, we can get the following control equations, which can be used to obtain the thermal post-buckling response.

For S-S

$$\begin{aligned} &\left[-\frac{\left(A_{66}L^2n^2+A_{11}\pi^2R^2m^2\right)}{L^2R^2}\right]\mathbf{U} \\ &+\left[\frac{\pi mn\left(B_{12}+2B_{66}+A_{12}R+A_{66}R\right)}{LR^2}\right]\mathbf{V} \\ &+\left[\pi m\begin{pmatrix}B_{12}L^2n^2+2B_{66}L^2n^2+A_{12}L^2R\\+B_{11}R^2m^2\pi^2\end{pmatrix}\frac{1}{L^3R^2}\right]\mathbf{W}=0 \end{aligned} \tag{17}$$

$$\begin{aligned} &\left[\frac{\pi mn\left(B_{12}+2B_{66}+A_{12}R+A_{66}R\right)}{LR^2}\right]\mathbf{U} \\ &-\left[\frac{1}{L^2R^4}\right]\begin{pmatrix}A_{22}L^2R^2n^2+2B_{22}L^2Rn^2+D_{22}L^2n^2\\+A_{66}\pi^2R^4m^2+4B_{66}\pi^2R^3m^2\\+4D_{66}\pi^2R^2m^2\end{pmatrix}\mathbf{V} \\ &-\left[\frac{1}{L^2R^4}\right]n\begin{pmatrix}D_{22}L^2n^2+B_{22}L^2R+A_{22}L^2R^2\\+B_{22}L^2Rn^2+B_{12}R^3m^2\pi^2\\+2B_{66}R^3m^2\pi^2+D_{12}R^3m^2\pi^2\\+4D_{66}R^2m^2\pi^2\end{pmatrix}\mathbf{W}=0 \end{aligned} \tag{18}$$

$$\begin{aligned} &\left[\frac{\pi m\left(B_{12}L^2n^2+2B_{66}L^2n^2+A_{12}L^2R+B_{11}R^2m^2\pi^2\right)}{L^3R^2}\right]\mathbf{U} \\ &-n\begin{pmatrix}D_{22}L^2n^2+B_{22}L^2R+A_{22}L^2R^2\\+B_{22}L^2Rn^2+B_{12}R^3m^2\pi^2+2B_{66}R^3m^2\pi^2\\+D_{12}R^3m^2\pi^2+4D_{66}R^2m^2\pi^2\end{pmatrix}\left[\frac{1}{L^2R^4}\right]\mathbf{V} \\ &-\begin{pmatrix}D_{22}L^4n^4+A_{22}L^4R^2+2B_{22}L^4Rn^2\\+D_{11}R^4m^4\pi^4+2B_{12}L^2R^3m^2\pi^2\\+L^2R^4m^2\pi^2ph-I_0L^2R^4V^2m^2\pi^2\\+4D_{66}L^2R^2m^2n^2\pi^2\end{pmatrix}\left[\frac{1}{L^4R^4}\right]\mathbf{W} \\ &+\begin{pmatrix}-\frac{3A_{22}W_1n^4}{16R^4}-\frac{3A_{11}W_1m^4\pi^4}{16L^4}-\frac{\pi A_{12}W_1m^2}{16L^2R}\\-\frac{3A_{12}W_1m^2n^2\pi^2}{16L^2R^2}+\frac{A_{66}W_1m^2n^2\pi^2}{4L^2R^2}\end{pmatrix}\mathbf{W}^2 \\ &+\begin{pmatrix}-96A_{22}L^4mn^5\pi^2\\-96A_{11}R^4m^5n\pi^6\\-192A_{12}L^2R^2m^3n^3\pi^4\\+128A_{66}L^2R^2m^3n^3\pi^4\end{pmatrix}\left[\frac{1}{1024L^4R^4mn\pi^2}\right]\mathbf{W}^3=0 \end{aligned} \tag{19}$$

For C-S

$$\begin{aligned} &\left[-\frac{\left(A_{66}L^2n^2+4A_{11}\pi^2R^2m^2\right)}{L^2R^2}\right]\mathbf{U} \\ &+\left[-\frac{2\pi mn\left(B_{12}+2B_{66}+A_{12}R+A_{66}R\right)}{LR^2}\right]\mathbf{V} \\ &+\frac{2mn\pi^2}{8L^3R^2n\pi}\left[\begin{pmatrix}B_{12}L^2n^2+2B_{66}L^2n^2\\+A_{12}L^2R+4B_{11}R^2m^2\pi^2\end{pmatrix}\right]\mathbf{W}=0 \end{aligned}$$

$$\begin{aligned} &\left[-\frac{2\pi mn\left(B_{12}+2B_{66}+A_{12}R+A_{66}R\right)}{LR^2}\right]\mathbf{U}+ \\ &\left[\begin{matrix}-\frac{6B_{22}n^2}{R^3}-\frac{3D_{22}n^2}{R^4}-\frac{4A_{66}m^2\pi^2}{L^2}-\frac{3A_{22}n^2}{R^2}\\-\frac{16B_{66}m^2\pi^2}{L^2R}-\frac{16D_{66}m^2\pi^2}{L^2R^2}\end{matrix}\right]\mathbf{V} \\ &+\left[\begin{matrix}\frac{A_{22}n}{R^2}+\frac{B_{22}n^3}{R^3}+\frac{3B_{22}n^3}{R^3}+\frac{3D_{22}n^3}{R^4}\\+\frac{16D_{66}m^2n\pi^2}{L^2R^2}+\frac{4D_{12}m^2n\pi^2}{L^2R}\\+\frac{8B_{66}m^2n\pi^2}{L^2R}+\frac{8B_{12}m^2n\pi^2}{L^2R}\end{matrix}\right]\mathbf{W}=0 \end{aligned}$$

$$\begin{aligned} &\frac{1}{8L^3R^2n\pi}\left[2mn\pi^2\begin{pmatrix}B_{12}L^2n^2+2B_{66}L^2n^2+A_{12}L^2R\\+4B_{11}R^2m^2\pi^2\end{pmatrix}\right]\mathbf{U} \\ &+\left[\begin{matrix}\frac{A_{22}n}{R^2}+\frac{B_{22}n^3}{R^3}+\frac{3B_{22}n^3}{R^3}+\frac{3D_{22}n^3}{R^4}+\frac{16D_{66}m^2n\pi^2}{L^2R^2}\\+\frac{4D_{12}m^2n\pi^2}{L^2R}+\frac{8B_{66}m^2n\pi^2}{L^2R}+\frac{8B_{12}m^2n\pi^2}{L^2R}\end{matrix}\right]\mathbf{V} \\ &+\left[\begin{matrix}\frac{2n^2B_{22}}{R^3}-\frac{16D_{11}m^4\pi^4}{L^4}-\frac{4m^2\pi^2ph}{L^2}+\frac{A_{22}}{R^2}\\+\frac{D_{22}n^4}{R^4}-\frac{8B_{12}m^2\pi^2}{L^2R}+\frac{4I_0V^2m^2\pi^2}{L^2}\\-\frac{16D_{22}m^2n^2\pi^2}{L^2R^2}-\frac{8D_{12}m^2n^2\pi^2}{L^2R^2}\end{matrix}\right]\mathbf{W} \\ &+\left[\begin{matrix}\frac{-60\pi B_{22}L^4mn^4+30\pi A_{22}L^4Rmn^2}{+96B_{12}L^2R^2m^3n^2\pi^3-96B_{66}L^2R^2m^3n^2\pi^3}\\36L^4R^4mn\pi^2\\-\frac{16\pi B_{66}m^2n}{3L^2R^2}-\frac{10B_{22}n^3}{3R^4\pi}-\frac{32B_{11}m^4\pi^3}{3L^4n}\\-\frac{10A_{22}n}{3R^3\pi}-\frac{32\pi B_{12}m^2n}{3L^2R^2}-\frac{16\pi A_{12}m^2}{3L^2Rn}\\+\frac{5\pi A_{12}W_1m^2}{16L^2R}-\frac{3A_{11}W_1m^4\pi^4}{L^4}-\frac{35A_{22}W_1n^4}{16R^4}\\-\frac{15A_{12}W_1m^2n^2\pi^2}{4L^2R^2}+\frac{5A_{66}W_1m^2n^2\pi^2}{L^2R^2}\end{matrix}\right]\mathbf{W}^2 \\ &+\left[\begin{matrix}-\frac{35A_{22}n^4}{32R^4}+\frac{3A_{11}m^4\pi^4}{2L^4}\\-\frac{13A_{12}m^2n^2\pi^2}{4L^2R^2}+\frac{5A_{66}m^2n^2\pi^2}{2L^2R^2}\end{matrix}\right]\mathbf{W}^3=0 \end{aligned} \tag{20}$$

5. Numerical analyses

In order to carry out the following research, firstly, a comparative analysis was carried out, as shown in Fig. 3, which can confirm the correctness of present paper. And the computing data in comparative analysis are (Liu *et al.* 2022): E_M=130 GPa, μ_M=0.34, ρ_M=8960 Kg/m^3, E_{gpl}=1010 GPa, μ_{gpl}=0.186, ρ_{gpl}=1060 Kg/m^3, L=d=2 m, h=0.1 m, α_{gpl} =2.35×10^{-5}/K, α_M =1.67×10^{-5}/K, e_1=0.6, W_{gpl}=0.01, and if there is no special description, the working condition is, m =1, n=2, L=2m, R = 0.4m, h=0.02m,W_{gpl}=0.01,e_1=0.4,GPL-B, Porosity- II.

In Fig. 4, we studied the influence of initial geometrical imperfections on the thermal post-buckling behavior of GPLRMF cylindrical shells. It can be seen from the figure that the initial geometrical imperfections have a significant influence on the thermal post-buckling behavior of cylindrical shells. When the initial geometrical defects do not exist, that is to say, w_1=0, thermal post buckling will not occur only until when the cylindrical shell reaches the critical buckling temperature; Whereas, when the cylindrical shell has initial geometrical defects, that is, $w_1 \neq 0$, as long as the temperature changes, the cylindrical shell will have a deflection, and the relationship curve between temperature and deflection is a parabola with the opening to the right. In addition, it should be noted that the deflection for the shells with geometrical defects are larger than those in the shells without geometrical defects. This is because defects will reduce the stiffness of the shell systems.

In Fig. 5, we studied the influence of the GPLs distribution types on the thermal post-buckling behavior of GPLRMF cylindrical shells. It can be seen that under different initial geometrical defect conditions, GPL-A cylindrical shells need the highest temperature for the occurrence of thermal post-buckling phenomenon, while GPL-B cylindrical shells need the lowest temperature to cause thermal post-buckling phenomenon, indicating that different GPLs distributions will affect the thermodynamic properties of shell structure.

In Fig. 6, we studied the influence of porosity distribution types on the thermal post-buckling behavior of GPLRMF cylindrical shells. It can be seen that from the perspective of porosity distribution types, in the case of

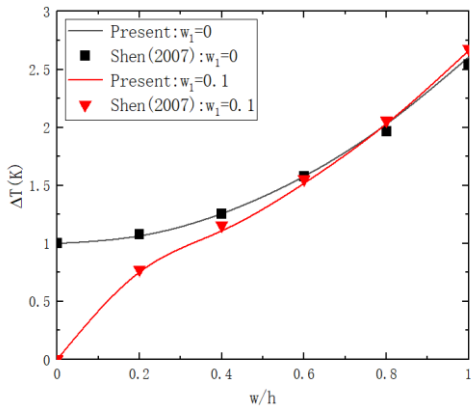

Fig. 3 Control study

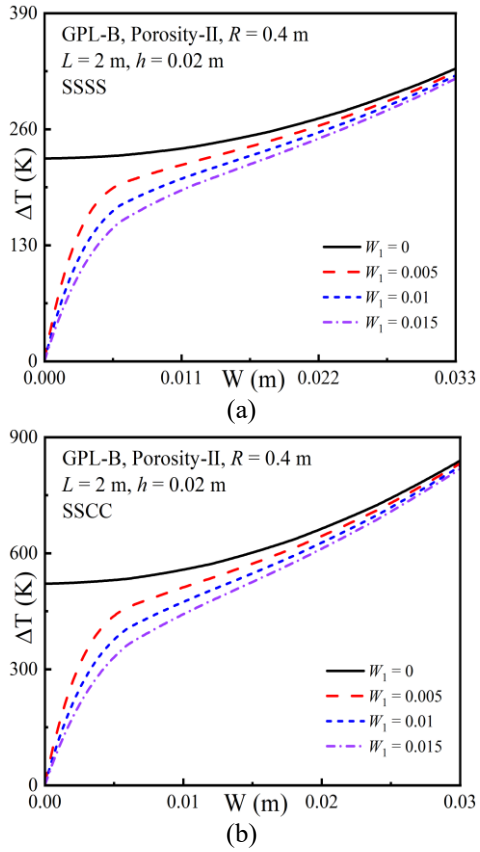

Fig. 4 Thermal post-buckling response for different initial geometrical imperfection

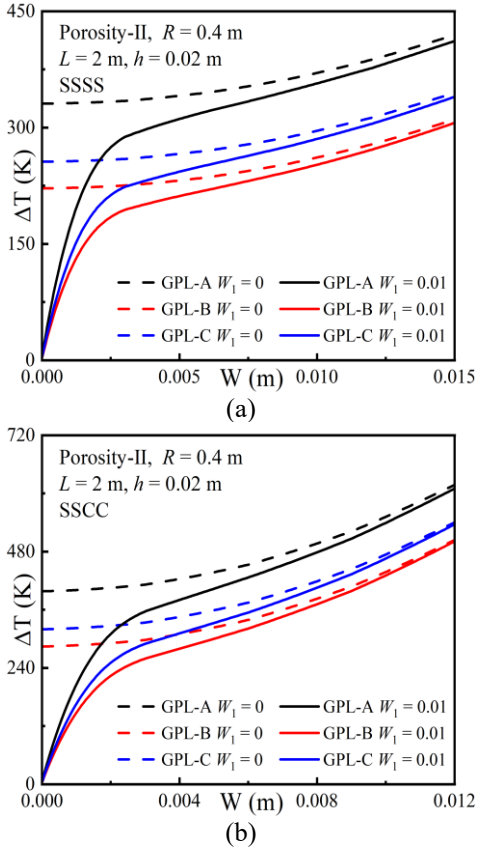

Fig. 5. Thermal post-buckling response for different GPLs distribution types

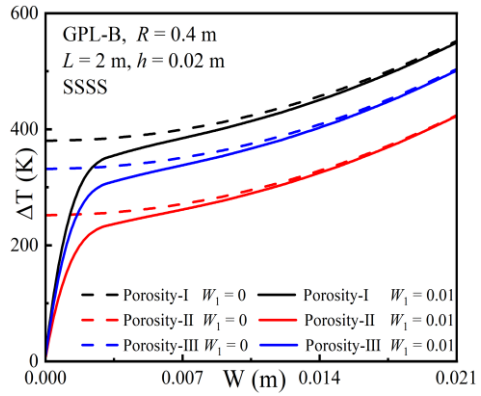

(a)

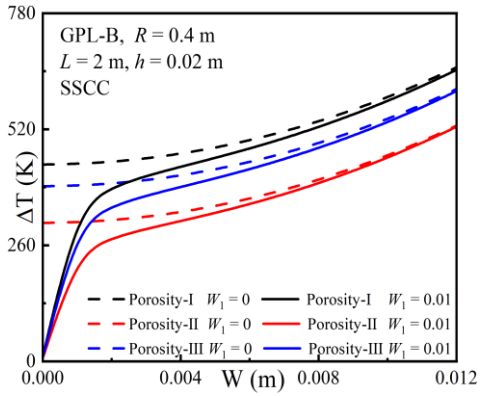

(b)

Fig. 6 Thermal post-buckling response for different porosity distribution types

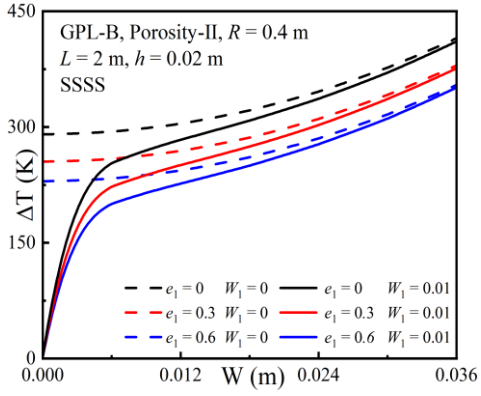

(a)

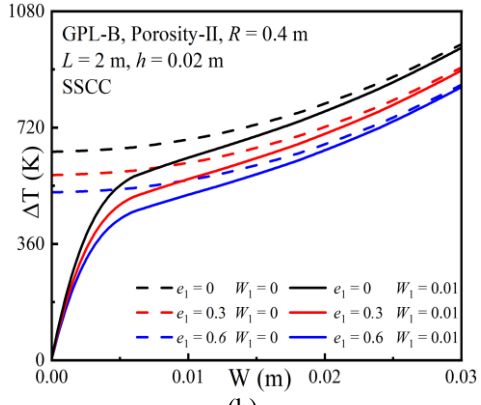

(b)

Fig. 7. Thermal post-buckling response for different porosity coefficient

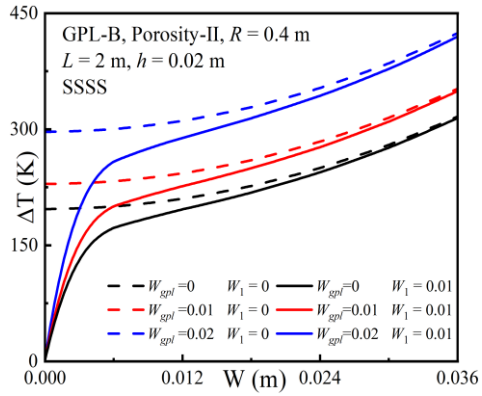

(a)

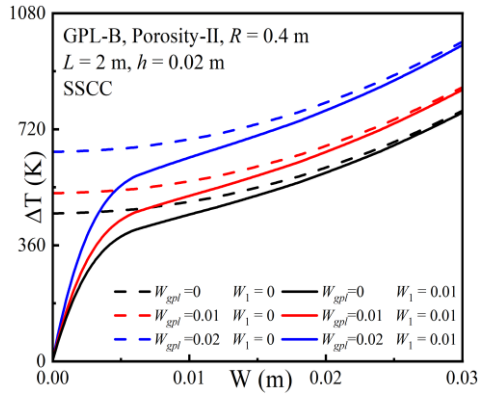

(b)

Fig. 8 Thermal post-buckling response for different GPLs mass fraction

same deflection, porosity -II and porosity -I have the lowest and highest thermal buckling temperatures respectively, and porosity -III is between them. That is, Porosity - I cylindrical shells need the highest temperature the thermal post-buckling phenomenon taking place, while Porosity - II cylindrical shells need the lowest temperature. Therefore, in order to obtain cylindrical shell structure with better performance, we suggest that the porosity distribution type should be set to Porosity - II when manufacturing the cylindrical shell structures.

In Fig. 7, we studied the influence of porosity coefficient on the thermal post-buckling behavior. When the porosity coefficient increases, the critical buckling temperature will also increase. Moreover, it is obvious that compared with cylindrical shell with S-S, the occurrence of thermal buckling of the cylindrical shell with C-S requires a higher buckling temperature when remaining other parameters unchanged.

In Fig. 8, we studied the influence of GPLs mass fraction. It can be seen that the greater the GPLs mass fraction, the larger the critical buckling temperature, suggesting that as the reinforcement of composite materials, GPLs can significantly improve the rigidity of the cylindrical shell, thus greatly increasing the critical buckling temperature of the cylindrical shell. Therefore, the introduction of GPLs is a good choice to improve the performance of the shell structure.

6. Conclusions

All the results are based on three different GPLs distribution patterns in this paper. The governing equation is acquired according to Eulerian-Lagrange equation. Meanwhile, Galerkin principle is applied to solve the governing equation. The effects of several parameters on the thermal post-buckling behavior of GPLRMF cylindrical shells are also investigated, including initial geometrical imperfections, porosity distribution types, porosity coefficient etc. The following results can be obtained:

(1) Thermal post-buckling will occur only the external temperature reaches critical buckling temperature as the cylindrical shell without initial geometrical imperfections. Conversely, the larger deflection will happen in the cylindrical shells with initial geometrical imperfections as long as the temperature changes.

(2) In the small deflection range, the thermal post-buckling temperature-deflection curve of the GPLRMF cylindrical shells without initial geometrical imperfections are always located above the GPLRMF cylindrical shells with initial geometrical imperfections, and the distance between these is gradually shortened with the increase of the deflection.

(3) GPL-B and GPL-A have the lowest and highest thermal buckling temperatures when the deflection changes are constant, and GPL-C is in between.

(4) Porosity -I has the greatest thermal buckling strength, while Porosity -I has the smallest one.

(5) In the situation of same external temperature changes, with the increase of the porosity coefficient, the deflection of the cylindrical shells also increases.

(6) When keeping the temperature increment unchanged, the larger the GPLs mass fraction is, the smaller the deflection change is.

References

Ahmadi, H., Bayat, A. and Duc, N.D. (2021), "Nonlinear forced vibrations analysis of imperfect stiffened FG doubly curved shallow shell in thermal environment using multiple scales method", *Compos. Struct.*, **256**, 113090. https://doi.org/10.1016/j.compstruct.2020.113090.

Akbari, M., Kiani, Y. and Eslami, M.R. (2015), "Thermal buckling of temperature-dependent FGM conical shells with arbitrary edge supports", *Acta. Mech.*, **226**(3), 897-915. https://doi.org/10.1007/s00707-014-1168-3.

Allahkarami, F. and Tohidi, H. (2022), "Axisymmetric postbuckling of functionally graded graphene platelets reinforced composite annular plate on nonlinear elastic medium in thermal environment", *Int. J. Struct. Stab. Dy.*, 2350034. https://doi.org/10.1142/S0219455423500347.

Alazwari, M.A., Daikh, A.A., Houari, M.S., Tounsi, A. and Eltaher, M.A. (2021), "On static buckling of multilayered carbon nanotubes reinforced composite nanobeams supported on non-linear elastic foundations", *Steel. Compos. Struct.*, **40**(3), 389-404. https://doi.org/10.12989/scs.2021.40.3.389.

Aris, H. and Ahmadi, H. (2022), "Combination resonance analysis of imperfect functionally graded conical shell resting on nonlinear viscoelastic foundation in thermal environment under multi-excitation", *J. Vib. Control.*, **28**(15-16), 2121-2144. https://doi.org/10.1177/10775463211006527.

Asadi, H., Kiani, Y., Aghdam, M.M. and Shakeri, M. (2016), "Enhanced thermal buckling of laminated composite cylindrical shells with shape memory alloy", *J. Compos. Mater.*, **50**(2), 243-256. https://doi.org/10.1177/0021998315573287.

Assie, A.E., Mohamed, S.A., Shanab, R.A., Abo-bakr, R.M. and Eltaher, M.A. (2023), "Static buckling of 2D FG porous plates resting on elastic foundation based on unified shear theories", *J. Appl. Comput. Mech.*, **9**(1), 239-258. https://doi.org/10.22055/jacm.2022.41265.3723.

Babaei, H. (2021), "On frequency response of FG-CNT reinforced composite pipes in thermally pre/post buckled configurations", *Compos. Struct.*, **276**, 114467. https://doi.org/10.1016/j.compstruct.2021.114467.

Babaei, H. (2022a), "Nonlinear analysis of size-dependent frequencies in porous FG curved nanotubes based on nonlocal strain gradient theory", *Eng. Struct.*, **38**(3), 1717-1734. https://doi.org/10.1007/s00366-021-01317-7.

Babaei, H. (2022b), "Free vibration and snap-through instability of FG-CNTRC shallow arches supported on nonlinear elastic foundation", *Appl. Math. Comput.*, **413**, 126606. https://doi.org/10.1016/j.amc.2021.126606.

Bagherizadeh, E., Kiani, Y. and Eslami, M.R. (2012), "Thermal buckling of functionally graded material cylindrical shells on elastic foundation", *Aiaa. J.*, **50**(2), 500-503. https://doi.org/10.2514/1.J051120.

Basha, M., Daikh, A.A., Melaibari, A., Wagih, A., Othman, R., Almitani, K.H., Hamed, M.A., Abdelrahman, A. and Eltaher, M.A. (2022), "Nonlocal strain gradient theory for buckling and bending of FG-GRNC laminated sandwich plates", *Steel. Compos. Struct.*, **43**(5), 639-660. https://doi.org/10.12989/scs.2022.43.5.639.

Boroujerdy, M.S., Naj, R. and Kiani, Y. (2014), "Buckling of heated temperature dependent fgm cylindrical shell surrounded by elastic medium", *J. Theor. App. Mech-Pol.*, **52**(4), 869-881.

Chen, X., Zhao, J.L., She, G.L., Jing, Y., Luo, J. and Pu, H.Y. (2022a), "On wave propagation of functionally graded CNT strengthened fluid-conveying pipe in thermal environment", *Eur. Phys. J. Plus.*, **137**(10), 1158. https://doi.org/10.1140/epjp/s13360-022-03234-0.

Chen, X., Zhao, J.L., She, G.L., Jing, Y., Pu, H.Y. and Luo, J. (2022b), "Nonlinear free vibration analysis of functionally graded carbon nanotube reinforced fluid-conveying pipe in thermal environment", *Steel. Compos. Struct.*, **45**(5), 641-652. https://doi.org/10.12989/scs.2022.45.5.641.

Dinis, P.B., Santana, K.G., Landesmann, A. and Camotim, D. (2021), "Numerical and experimental study on CFS spherically-hinged equal-leg angle columns: stability, strength and DSM design", *Thin. Wall. Struct.*, **161**, 106862. https://doi.org/10.1016/j.tws.2020.106862.

Ding, H.X. and She, G.L. (2021), "A higher-order beam model for the snap-buckling analysis of FG pipes conveying fluid", *Struct. Eng. Mech.*, **80**(1), 63-72. https://doi.org/10.12989/sem.2021.80.1.063.

Ding, H.X., She, G.L. and Zhang, Y.W. (2022a), "Nonlinear buckling and resonances of functionally graded fluid-conveying pipes with initial geometric imperfection", *Eur. Phys. J. Plus*, **137**,1329. https://doi.org/10.1140/epjp/s13360-022-03570-1.

Ding, H.X., Zhang, Y.W. and She, G.L. (2022b), "On the resonance problems in FG-GPLRC beams with different boundary conditions resting on elastic foundations", *Comput. Concrete*, **30**(6), 433-443. https://doi.org/10.12989/cac.2022.30.6.433.

Ebrahimi, F., Nouraei, M. and Dabbagh, A. (2020), "Modeling vibration behavior of embedded graphene-oxide powder-reinforced nanocomposite plates in thermal environment", *Mech. Based. Des. Struc.*, **48**(2), 217-240. https://doi.org/10.1080/15397734.2019.1660185.

Eltaher, M. A., Mohamed, N., Mohamed, S.A. and Seddek, L.F. (2019a), "Periodic and nonperiodic modes of postbuckling and nonlinear vibration of beams attached to nonlinear foundations",

Appl. Math. Model., **75**, 414-445. https://doi.org/10.1016/j.apm.2019.05.026.

Eltaher, M.A., Mohamed, N., Mohamed, S.A. and Seddek, L.F. (2019b), "Postbuckling of curved carbon nanotubes using energy equivalent model", *J. Nano Res*., **57**, 136-157. https://doi.org/10.4028/www.scientific.net/JNanoR.57.136.

Gholami, R. and Ansari, R. (2019), "Nonlinear stability and vibration of pre/post-buckled multilayer FG-GPLRPC rectangular plates", *Appl. Math. Model*., **65**, 627-660. https://doi.org/10.1016/j.apm.2018.08.038.

Gao, K., Gao, W., Chen, D. and Yang, J. (2018), "Nonlinear free vibration of functionally graded graphene platelets reinforced porous nanocomposite plates resting on elastic foundation", *Compos. Struct*., **204**, 831-846. https://doi.org/10.1016/j.compstruct.2018.08.013.

Hendi, A., Eltaher, M.A, Mohamed, S.A. and Attia, M. (2022), "Nonlinear thermal vibration of pre/post-buckled two-dimensional FGM tapered microbeams based on a higher order shear deformation theory", *Steel Compos. Struct*., **41**(6), 787-802. http://doi.org/DOI10.12989/scs.2021.41.6.787.

Ismail, M.S., Ifayefunmi, O., Fadzullah, S.H.S.M. and Johar, M. (2020), "Buckling of imperfect cone-cylinder transition subjected to external pressure", *Int. J. Pres. Ves. Pip*., **187**, 104173. https://doi.org/10.1016/j.ijpvp.2020.104173.

Javani, M., Kiani, Y. and Eslami, M.R. (2020), "Thermal buckling of FG graphene platelet reinforced composite annular sector plates", *Thin. Wall. Struct*., **148**, 106589. https://doi.org/10.1016/j.tws.2019.106589.

Kiani, Y. (2020), "NURBS-based thermal buckling analysis of graphene platelet reinforced composite laminated skew plates", *J. Therm. Stresses*., **43**(1), 90-108. https://doi.org/10.1080/01495739.2019.1673687.

Kolahchi, R., Hosseini, H., Fakhar, M.H., Taherifar, R. and Mahmoudi, M. (2019), "A numerical method for magneto-hygro-thermal post-buckling analysis of defective quadrilateral graphene sheets using higher order nonlocal strain gradient theory with different movable boundary conditions", *Comput. Math. Appl*., **78**(6), 2018-2034. https://doi.org/10.1016/j.camwa.2019.03.042.

Krasovsky, V. and Evkin, A. (2021), "Experimental investigation of buckling of dented cylindrical shells under axial compression", *Thin. Wall. Struct*., **164**, 107869. https://doi.org/10.1016/j.tws.2021.107869.

Khaniki, H.B., Ghayesh, M.H., Hussain, S. and Amabili, M. (2022), "Porosity, mass and geometrical imperfection sensitivity in coupled vibration characteristics of CNT-strengthened beams with different boundary conditions", *Eng. Comput-Germany*., **38**(3), 2313-2339. https://doi.org/10.1007/s00366-020-01208-3.

Kolakowski, Z., Kubiak, T., Zaczynska, M. and Kazmierczyk, F. (2020), "Global-distortional buckling mode influence on post-buckling behaviour of lip-channel beams", *Int. J. Mech. Sci*., **184**, 105723. https://doi.org/10.1016/j.ijmecsci.2020.105723.

Liu, Y.F., Hu, W.Y., Zhu, R., Safaei, B., Qin, Z.Y. and Chu, F.L. (2022), "Dynamic responses of corrugated cylindrical shells subjected to nonlinear low-velocity impact", *Aerosp. Sci. Technol*., **121**, 107321.https://doi.org/10.1016/j.ast.2021.107321.

Lu, L., She, G.L. and Guo, X. (2021), "Size-dependent postbuckling analysis of graphene reinforced composite microtubes with geometrical imperfection", *Int. J. Mech. Sci*., **199**, 106428. https://doi.org/10.1016/j.ijmecsci.2021.

Ma, Y., Martinez-Vazquez, P. and Baniotopoulos, C. (2020), "Buckling analysis for wind turbine tower design: Thrust load versus compression load based on energy method", *Energies*, **13**(20), 5302. https://doi.org/10.3390/en13205302.

Malikan, M., Tornabene, F. and Dimitri, R. (2019), "Transient response of oscillated carbon nanotubes with an internal and external damping", *Compos. Part B: Eng*., **158**, 198-205. https://doi.org/10.1016/j.compositesb.2018.09.092.

Malikan, M., Wiczenbach, T. and Eremeyev, V.A. (2022), "Thermal buckling of functionally graded piezomagnetic micro- and nanobeams presenting the flexomagnetic effect", Continuum Mech. Thermodynam., **34**(4), 1051-1066. https://doi.org/10.1007/s00161-021-01038-8.

Mahani, R.B., Eyvazian, A., Musharavati, F., Sebaey, T.A. and Talebizadehsardari, P. (2020), "Thermal buckling of laminated Nano-Composite conical shell reinforced with graphene platelets", *Thin. Wall. Struct*., **155**, 106913. https://doi.org/10.1016/j.tws.2020.106913.

Martins, A.D., Goncalves, R. and Camotim, D. (2021), "Post-buckling behaviour of thin-walled regular polygonal tubes subjected to bending", *Thin. Wall. Struct*., **166**, 108106. https://doi.org/10.1016/j.tws.2021.108106.

Martins, A.D. and Silvestre, N. (2020), "Modal analysis and imperfection sensitivity of the post-buckling behaviour of cylindrical steel panels under in-plane bending", *Eng. Struct.*, **207**, 110127. https://doi.org/10.1016/j.engstruct.2019.110127.

Martins, A.D., Goncalves, R. and Camotima, D. (2019), "Post-buckling behaviour of thin-walled regular polygonal tubular columns undergoing local-distortional interaction", *Thin. Wall. Struct*., **138**, 373-391. https://doi.org/10.1016/j.tws.2019.02.020.

Melaibari, A., Mohamed, S.A., Assie, A.E., Shanab, R.A. and Eltaher, M.A. (2023), "Static response of 2D FG porous plates resting on elastic foundation using midplane and neutral surfaces with movable constraints", *Mathematics*, **10**(24), 4784. https://doi.org/10.3390/math10244784.

Ming, S.Z., Song, Z.B., Zhou, C.H., Li, T., Du, K.F., Xu, S.L. and Wang, B. (2021), "The energy absorption of long origami-ending tubes with geometrical imperfections", *Thin. Wall. Struct*., **161**, 107415. https://doi.org/10.1016/j.tws.2020.107415.

Mirjavadi, S.S., Forsat, M., Barati, M.R. and Hamouda, A.M.S. (2020), "Post-buckling of higher-order stiffened metal foam curved shells with porosity distributions and geometrical imperfection", *Steel. Compos. Struct*., **35**(4), 567-578. https://doi.org/10.12989/scs.2020.35.4.567.

Mohamed, N., Mohamed, S.A. and Eltaher, M. A. (2021), "Buckling and post-buckling behaviors of higher order carbon nanotubes using energy-equivalent model", *Eng. with Comput*., **37**(4), 2823-2836. http://dx.doi.org/10.1007/s00366-020-00976-2.

Mohamed, N., Eltaher, M.A., Mohamed, S.A. and Seddek, L.F. (2019), "Energy equivalent model in analysis of postbuckling of imperfect carbon nanotubes resting on nonlinear elastic foundation", *Struct. Eng. Mech*., **70**(6), 737-750. https://doi.org/10.12989/sem.2019.70.6.737.

Nguyen, T.P., Vu, M.D., Cao, V.D. and Vu, H.N. (2021), "Nonlinear torsional buckling of functionally graded graphene-reinforced composite (FG-GRC) laminated cylindrical shells stiffened by FG-GRC laminated stiffeners in thermal environment", *Polym. Compos*., **42**(6), 3051-3063. https://doi.org/10.1002/pc.26038.

Phuong, N.T., Trung, N.T., Doan, C.V., Thang, N.D., Duc, V.M. and Nam, V.H. (2020), "Nonlinear thermomechanical buckling of FG-GRC laminated cylindrical shells stiffened by FG-GRC stiffeners subjected to external pressure", *Acta. Mech*., **231**(12), 5125-5144. https://doi.org/10.1007/s00707-020-02813-5.

Phuong, N.T., Dong, D.T., Van Doan, C. and Nam, V.H. (2022), "Nonlinear buckling of higher-order shear deformable stiffened FG-GRC laminated plates with nonlinear elastic foundation subjected to combined loads", *Aerosp. Sci. Technol*., **127**, 107736. https://doi.org/10.1016/j.ast.2022.107736.

Phuong, N.T., Nam, V.H., Trung, N.T., Duc, V.M., Loi, N.V., Thinh, N.D. and Tu, P.T. (2021), "Thermomechanical postbuckling of functionally graded graphene-reinforced composite laminated toroidal shell segments surrounded by Pasternak's elastic foundation", *J. Thermoplast. Compos*., **34**(10), 1380-1407. https://doi.org/10.1177/0892705719870593.

Quyen, N.V., Thanh, N.V., Quan, T.Q. and Duc, N.D. (2021),

"Nonlinear forced vibration of sandwich cylindrical panel with negative Poisson's ratio auxetic honeycombs core and CNTRC face sheets", *Thin. Wall. Struct*., **162**, 107571. https://doi.org/10.1016/j.tws.2021.107571.

Ramezani, M., Rezaiee-Pajand, M. and Tornabene, F. (2022), "Nonlinear thermomechanical analysis of GPLRC cylindrical shells using HSDT enriched by quasi-3D ANS cover functions", *Thin. Wall. Struct*., **179**, 109582. https://doi.org/10.1016/j.tws.2022.109582.

Saiah, B., Bachene, M., Guemana, M., Chiker, Y. and Attaf, B. (2022), "On the free vibration behavior of nanocomposite laminated plates contained piece-wise functionally graded graphene-reinforced composite plies", *Eng. Struct*., **253**, 113784. https://doi.org/10.1016/j.engstruct.2021.113784.

Sahmani, S., Aghdam, M.M. and Rabczuk, T. (2018), "Nonlinear bending of functionally graded porous micro/nano-beams reinforced with graphene platelets based upon nonlocal strain gradient theory", *Compos. Struct*., **186**, 68-78. https://doi.org/10.1016/j.compstruct.2017.11.082.

Shahgholian, D., Safarpour, M., Rahimi, A.R. and Alibeigloo, A. (2020), "Buckling analyses of functionally graded graphene-reinforced porous cylindrical shell using the Rayleigh-Ritz method", *Acta. Mech*., **231**(5), 1887-1902. https://doi.org/10.1007/s00707-020-02616-8.

Shahgholian-Ghahfarokhi, D., Rahimi, G., Khodadadi, A., Salehipour, H. and Afrand, M. (2021), "Buckling analyses of FG porous nanocomposite cylindrical shells with graphene platelet reinforcement subjected to uniform external lateral pressure", *Mech. Based. Des. Struc*., **49**(7), 1059-1079. https://doi.org/10.1080/15397734.2019.1704777.

Salehi, M., Gholami, R. and Ansari, R. (2022), "Nonlinear resonance of functionally graded porous circular cylindrical shells reinforced by graphene platelet with initial imperfections using higher-order shear deformation theory", *Int. J. Struct. Stab. Dy*., **22**(6), 2250075. https://doi.org/10.1142/S0219455422500754.

Stawiarski, A., Chwal, M., Barski, M. and Muc, A. (2020), "The influence of the manufacturing constraints on the optimal design of laminated conical shells", *Compos. Struct.*, **235**, 111820. https://doi.org/10.1016/j.compstruct.2010.111820.

She, G.L. (2020), "Wave propagation of FG polymer composite nanoplates reinforced with GNPs", *Steel Compos. Struct*., **37**(1) , 27-35. https://doi.org/10.12989/scs.2020.37.1.027.

She, G.L. (2021), "Guided wave propagation of porous functionally graded plates: The effect of thermal loadings", *J. Therm. Stresses*., **44**(10), 1289-1305. https://doi.org/10.1080/01495739.2021.1974323.

She, G.L. and Ding, H.X. (2023), "Nonlinear primary resonance analysis of initially stressed graphene platelet reinforced metal foams doubly curved shells with geometric imperfection", *Acta Mech. Sin*., **39**, 522392. https://doi.org/10.1007/s10409-022-22392-x.

She, G.L., Ding, H.X. and Zhang, Y.W. (2022), "Wave propagation in a FG circular plate via the physical neutral surface concept", *Struct. Eng. Mech*., **82**(2), 225-232. https://doi.org/10.12989/sem.2022.82.2.225.

She, G.L. and Li, Y.P. (2022), "Wave propagation in an FG circular plate in thermal environment", *Geomech. Eng*., **31**(6), 615-622. https://doi.org/10.12989/gae.2022.31.6.615.

She, G.L., Liu, H.B. and Karami, B. (2021), "Resonance analysis of composite curved microbeams reinforced with graphene nanoplatelets", *Thin Wall. Struct*., **160**, 107407. https://doi.org/10.1016/j.tws.2020.107407.

Shen, H.S. (2007), "Thermal postbuckling behavior of shear deformable FGM plates", *Int. J. Mech. Sci*., **49**(4), 466-478.https://doi.org/10.1016/j.ijmecsci.2006.09.011.

Trang, L.T.N. and Tung, H.V. (2022), "Thermally induced post-buckling of thin CNT-reinforced composite plates under nonuniform in-plane temperature distributions", *J. Thermoplast. Compos*., **35**(12), 2331-2353. https://doi.org/10.1177/0892705720962172

Torabi, J., Kiani, Y. and Eslami, M.R. (2013), "Linear thermal buckling analysis of truncated hybrid FGM conical shells", *Compos. Part B-Eng*., **50**, 265-272. https://doi.org/10.1016/j.compositesb.2013.02.025.

Van Doan, C., Hung, V.T., Phuong, N.T. and Nam, V.H. (2022), "Torsional buckling and postbuckling behavior of stiffened FG-GRCL toroidal shell segments surrounded by elastic foundation", *Int. J. Comput. Mat. Sci*., 2350001. https://doi.org/10.1142/S204768412350001X.

Wang, Y. and Wu, D. (2017), "Free vibration of functionally graded porous cylindrical shell using a sinusoidal shear deformation theory", *Aerosp. Sci. Technol*., **66**, 83-91. https://doi.org/10.1016/j.ast.2017.03.003.

Wang, Y., Xie, K., Fu, T. and Shi, C. (2019), "Vibration response of a functionally graded graphene nanoplatelet reinforced composite beam under two successive moving masses", *Compos. Struct*., **209**, 928-939.https://doi.org/10.1016/j.compstruct.2018.11.014.

Wu, H.L., Kitipornchai, S. and Yang, J. (2017), "Thermal buckling and postbuckling of functionally graded graphene nanocomposite plates", *Mater. Design*, **132**, 430441. https://doi.org/10.1016/j.matdes.2017.07.025.

Xu, J.Q. and She, G.L. (2022), "Thermal post-buckling analysis of porous functionally graded pipes with initial geometric imperfection", *Geomech. Eng*., **31**(3), 329-337. https://doi.org/10.12989/gae.2022.31.3.329.

Yilmaz, H., Ozyurt, E., Onder, A. and Tomek, P. (2020), "Elastic limit load estimation including similarity approach for different end conditioned conical shells with high semi-vertex angle under axial compression", *Thin. Wall. Struct*., **149**, 106543. https://doi.org/10.1016/j.tws.2019.106543.

Zhang, Y.W., Ding, H.X. and She, G.L. (2022), "Snap-buckling and resonance of functionally graded graphene reinforced composites curved beams resting on elastic foundations in thermal environment", *J. Therm. Stresses*, **45**(12), 1029-1042.https://doi.org/10.1080/01495739.2022.2125137.

Zhang, Y.W., Ding, H.X. and She, G.L. (2023a), "Wave propagation in spherical and cylindrical panels reinforced with carbon nanotubes", *Steel Compos. Struct*., **46**(1),133-141. https://doi.org/10.12989/scs.2023.46.1.133.

Zhang, Y.W., She, G.L. and Ding, H.X. (2023b), "Nonlinear resonance of graphene platelets reinforced metal foams plates under axial motion with geometric imperfections", *Eur. J. Mech. A-Solid*., **98**, 104887. https://doi.org/10.1016/j.euromechsol.2022.104887.

Zhang, Y.W. and She, G.L. (2022), "Wave propagation and vibration of FG pipes conveying hot fluid", *Steel. Compos, Struct*., **42**(3) 397-405. https://doi.org/10.12989/scs.2022.42.3.397.

Zhang, Y.W. and She, G.L. (2023a), "Nonlinear low-velocity impact response of graphene platelet-reinforced metal foam cylindrical shells under axial motion with geometrical imperfection", *Nonlinear Dynam*., https://doi.org/10.1007/s11071-022-08186-9.

Zhang, Y.W. and She, G.L. (2023b), "Nonlinear primary resonance of axially moving functionally graded cylindrical shells in thermal environment", *Mech. Adv. Mater. Struct*., https://doi.org/10.1080/15376494.2023.2180556.

Zhang, Y.Y., Wang, X.Y., Zhang, X., Shen, H.M. and She, G.L. (2021), "On snap-buckling of FG-CNTRC curved nanobeams considering surface effects", *Steel Compos. Struct*., **38**(3), 293-304. https://doi.org/10.12989/scs.2021.38.3.293.

Zhao, J.L., Chen, X., She, G.L., Jing, Y., Bai, R.Q., Yi, J., Pu, H.Y. and Luo, J. (2022a), "Vibration characteristics of functionally graded carbon nanotube-reinforced composite double-beams

in thermal environments", *Steel. Compos. Struct*., **43**(6), 797-808. https://doi.org/10.12989/scs.2022.43.6.797.

Zhao, J.L., She, G.L., Wu, F., Yuan, S.J., Bai, R.Q., Pu, H.Y., Wang, S.L. and Luo, J. (2022b), "Guided waves of porous FG nanoplates with four edges clamped", *Adv. Nano. Res*., **13**(5), 465-474. https://10.12989/anr.2022.13.5.465.

Zmuda-Trzebiatowski, L. and Iwicki, P. (2021), "Impact of geometrical imperfections on estimation of buckling and limit loads in a silo segment using the vibration correlation technique", *Materials*, **14**(3), 567. https://doi.org/10.3390/ma14030567.

CC